Specular Reflectance (SR) and Attenuated Total Reflectance (ATR) Infrared (IR) Spectroscopy of Transparent Flat Glass Surfaces: A Case Study for Soda Lime Float Glass

Shin-ichi Amma,[a,b,] Jiawei Luo,[c] Carlo G. Pantano,[a] and Seong H. Kim[a,c*]

a) Materials Research Institute, Department of Materials Science and Engineering, Pennsylvania State University, University Park, PA, 16802, USA.

b) Research Center, Asahi Glass Co., Ltd., 1150 Hazawa-cho, Kanagawa-ku, Yokohama-shi, Kanagawa, 221-8755, Japan.

c) Department of Chemical Engineering, Pennsylvania State University, University Park, PA, 16802, USA.

* Corresponding author: shkim@engr.psu.edu

Abstract: This paper describes the optical principles of specular reflection (SR) and attenuated total reflection (ATR) - infrared (IR) spectroscopy, both of which are useful methods for glass surface analyses. It should be noted that the shape, position, and relative intensity of peaks in reflectance spectra vary drastically depending on the IR incidence angle as well as the probe method (SR vs. ATR). For example, in SR-IR analyses of soda lime glass, the Si-O-Si stretch band shows a blue-shift from its original position and a new peak grows at ~1200 cm^{-1} as the IR incidence angle increases. In contrast, the Si-O-Si stretch band appears be significantly red-shifted from its original position in the ATR-IR spectra of soda lime glass. SR-IR spectra of

thin and flat samples can contain transmission spectral features, due to the reflection from the backside, in the region where the bulk absorption coefficient is low. These artifacts are due to the complex nature of refractive index and should not be interpreted as new peaks or new chemical states of soda lime glass surfaces. An ATR-IR analysis to probe hydrous species in glass surface is demonstrated using two ATR crystals with different refractive indices.

Keywords: soda-lime glass, infrared spectroscopy, specular reflectance, attenuated total reflectance, hydrous species.

1. Introduction

For silicate glasses, mechanical strength and chemical reactivity are known to be affected by its surface condition, especially the speciation and concentration of hydrous species (Si-OH or H_2O) and the network structure (Si-O-Si bridging oxygen (BO) and Si-O^- non-bridging oxygen (NBO)) [1,2]. For example, distributions of these groups can affect surface corrosion [3,4], adhesion of coatings [5,6], and fictive temperature [7] of silicate glasses. Therefore, full characterization of the chemical structure of the surface and subsurface region of silicate glass is very important. Among various surface-sensitive analytical techniques, infrared (IR) spectroscopy has been widely used for this purpose. IR can probe BO and NBO groups, as well as Si-OH and H_2O species inside the glass [3–7].

In order to obtain surface information, IR analysis of glass must be carried out in a specular reflection (SR) or attenuated total reflection (ATR) configuration, rather than typical transmission mode [8]. Figure 1 schematically compares these three methods. In the transmission mode, the signal intensity is often expressed as absorbance (A) which is defined as $-\log(I_t/I_o)$ where I_o and I_t are the intensities of the incident and transmitted IR beams, respectively. The absorbance follows the Beer-Lambert law, $A = abc$ where a is specific absorptivity, b is sample thickness, and c is concentration of the species of interest. Since the thickness of the surface region affected by glass manufacturing processes or environmental corrosion is much

thinner than the total thickness of the sample ($b_{surface} << b_{bulk}$), the transmission signal is always dominated by bulk species and their structure.

In SR-IR, the intensity of the reflected beam (I_r) is measured and expressed as a reflectance ($R=I_r/I_o$), which is *dimensionally equivalent* to the transmittance (I_t/I_o) in the transmission mode experiment. When the IR frequency resonates with the absorption band of the sample, the reflected beam intensity is enhanced in SR-IR. Thus, the peak in the R vs. wavenumber (cm^{-1}) plot of SR-IR is positive, while the peak in transmission IR is negative when plotted in the percent transmission ($I_t/I_o \times 100\%$) scale.

In the case of ATR-IR, a crystal with a refractive index (n_1) higher than that of sample of interest (n_2) is in intimate contact with the sample surface and the IR probe beam is irradiated through this crystal. When the IR incidence angle (θ_i) is higher than the critical angle ($\theta_c=\arcsin(n_2/n_1)$), then the IR beam is totally reflected from the crystal/sample interface and only an evanescent wave penetrates into the sample. The interaction of this evanescent wave and the absorption band of the sample attenuates the total reflection. When the measured reflectance (R) is plotted as log(1/R), then it is *dimensionally equivalent* to the absorbance; thus, peaks in ATR-IR spectra are often interpreted as absorption bands as in the case of transmission spectra.

However, it should be noted that peaks in the transmission IR spectra are governed by the absorptivity (a) which is a function of the imaginary (k) part of the complex refractive index of

glass (n+ik) [i.e., $a = 4\pi k/\lambda$ where λ is the IR wavelength], while those in the SR-IR and ATR-IR spectra are governed by both the real (n) and imaginary (k) parts that vary over a large range [9]. As shown in Figure 2 [9], the real part of the glass refractive index is not constant; due to the Kronig-Kramers relationship, [10,11] n varies significantly along with k especially near the absorption band region. Thus, the SR-IR and ATR-IR spectra of glass cannot be interpreted in the same manner as the transmission IR peaks. The peak position, shape, and relative intensity can be drastically different in the SR-IR and ATR-IR spectra of glass.

Although ATR-IR spectroscopy is a useful and convenient method for evaluation of glass surface because it can be more surface sensitive than transmission IR analysis, only few studies on ATR-IR for inorganic glasses have been reported [12–15] and none of them discussed the comparison between theoretical and experimental spectra from glass surface. This paper aims to provide clear explanations of how the spectral features in both SR-IR and ATR-IR spectra of glass are altered at various measurement conditions and how they should be interpreted. These spectral effects are discussed for as-produced float glass and acid treated soda lime glass; the same principles can be applied to other types of glass.

2. Experimental methods

2.1 Sample preparation

Soda lime float glasses (0.7mm-thick) were used in this study as as-produced sample, which were supplied by Asahi Glass Co. Ltd. in Japan. The bulk composition of the glasses was analyzed by x-ray fluorescence (XRF) and is shown in Table 1. In all reflection experiments, the air-side of the float glass was used as the top side where incident IR beam entered. Some float glass samples were remelted in a Pt crucible in an electric furnace and quenched on a carbon plate. The quenched glass blocks were annealed at 600 ^{o}C for 1 hour and cooled slowly at a cooling rate of 1 ^{o}C/min to remove residual stress. Annealed glasses were then cut and polished with SiC sandpaper and CeO_2 dispersed in water into 5.0 mm thick slabs. Before IR measurements, all samples were cleaned with distilled water and ethanol in an ultrasonic cleaner and then using an UV/ozone cleaner.

In order to study changes in the hydrous species and the glass network structure in the surface region, the remelted and polished glass samples were treated with a 0.1M HCl solution at 90 ^{o}C for 1, 5, 20, 80, and 320 hours. The surface area of each sample treated with 50ml HCl solution was 7.5 cm^2. The hydrogen depth profiles in the acid-treated sample surface were previously analyzed with secondary-ion mass spectroscopy (SIMS) and reported elsewhere [15].

Table 1. Glass composition determined by XRF

	SiO_2	Al_2O_3	MgO	CaO	Na_2O	K_2O	Fe_2O_3
mol%	70.8	1.0	6.2	9.1	12.5	0.4	0.04

2.2 SR-IR measurements

SR-IR spectra of both as-produced float glass with 0.7 mm thickness and polished and leached samples with 5.0 mm thickness were obtained by three instruments: (i) 20^o incidence angle from the surface normal direction using a Bruker Hyperion 3000 micro-FT-IR system equipped with a 15x infrared microscope objective lens (Bruker Optics Inc.), (ii) ~45^o incidence angle using a Thermo-Nicholet 670 FTIR system equipped with a custom-arranged optics, and (iii) 43^o, 53^o, 58^o, 63^o, and 68^o incidence angles using a Bruker Hyperion 3000 system equipped with a Pike VeeMAX II ATR accessory. SR-IR spectra were obtained in the range of 4000 – 500 cm^{-1}. Spectra were acquired for three spots per sample in 400 scan passes at a 4 cm^{-1} resolution. A gold mirror was used as a standard reference for all measurements.

2.3 ATR-IR measurements

A Bruker Vertex70 FT-IR system was used for ATR-IR analysis of both float (0.7mm thickness) and leached (5.0mm thickness) soda-lime glass samples using diamond and Ge ATR crystals. For the diamond ATR (MVP-Pro, Harrick Scientific Products), the IR beam incident angle was 45°. The sample was contacted against the ATR diamond crystal with a force of

pushed by 420 N over a 1.5 mm^2 sampling area. For the Ge ATR (VariGATR, Harrick Scientific Products), the IR incident angle was set at 60^o. The sample was contacted against the ATR germanium crystal with a force of pushed by 600 N over 1 cm^2 sampling area. Spectra were collected for 100 scans with a spectral resolution of 6 cm^{-1} from 4000 to 400 cm^{-1} for diamond ATR and from 4000 to 800 cm^{-1} in Ge ATR. The diamond ATR crystal absorbs IR in the 2300 and 2000 cm^{-1} region; so, this region cannot be probed. For the same reason, the Ge ATR-IR spectrum cuts off at 800 cm^{-1}. For quantitative comparison of water related species as a function of acid treatment time, the peak intensity at 3400cm^{-1} was plotted after background correction.

2.4 Simulations of SR- and ATR- IR spectra

The reflectance of the IR beam was calculated using the Fresnel equations [16] and the refractive index of soda lime glass was taken from a literature (Figure 2) [9]. The reflection coefficients of *p*-polarized and *s*-polarized beams (r_p and r_s, respectively) at an interface between media 1 and 2 are expressed as:

$$r_{p,12} = \frac{n_2 cos\theta_1 - n_1 cos\theta_2}{n_2 cos\theta_1 + n_1 cos\theta_2} \quad \text{and} \quad r_{s,12} = \frac{n_1 cos\theta_1 - n_2 cos\theta_2}{n_1 cos\theta_1 + n_2 cos\theta_2} \qquad (1)$$

where n_1 is the refractive index of the media 1, n_2 is the complex refractive index of media 2 ($n_2 = n(\lambda) + ik(\lambda)$ from Figure 2 [9]), θ_1 is the incident angle (θ_i in Figure 1) and θ_2 is the transmission angle (θ_t in Figure 1) calculated from Snell's equation: $n_1 sin\theta_1 = n_2 sin\theta_1$. In the case of SR-IR, n_1 = 1 (air); in the case of ATR-IR, n_1 = ~2.4 diamond and ~4 for germanium. The

exact n_1 value as a function of IR wavenumber can be found at [17] for diamond and [18] for germanium. Then, the reflectance of p-polarized (electric vector polarized parallel to the incidence plane) and s-polarized (perpendicular to the incidence plane) component of the IR beam are calculated as:

$$R_p = r_{p,12} r_{p,12}^* \text{ and } R_s = r_{s,12} r_{s,12}^* \quad (2)$$

and the total reflectance of the unpolarized beam is the average of these two values:

$$R = \left(R_p + R_s\right)/2 \quad (3)$$

Within the glass sample, the electric filed intensity of IR decreases with an exponential function of the distance from the surface. The characteristic attenuation or penetration distance is expressed as the distance required for the electric field amplitude (transmitted beam in SR-IR or evanescent wave in ATR-IR) to fall to 36.8% (e^{-1}) of its value at the surface. The penetration of depth of SR-IR is defined as $d_{p,SR} = \lambda/4\pi k(\lambda)$ [3]. The penetration depth in ATR-IR is expressed as $d_{p,ATR} = \lambda/\left(2\pi \mathrm{Im}\left[\sqrt{n_2^2 - n_1^2 sin^2\theta_1}\right]\right)$ where Im[] means the magnitude of the imaginary part.[19] Note that when $k(\lambda) \approx 0$, then $d_{p,ATR}$ can be calculated using only the real part of n_2. The information depth from which most of IR signal comes from is three times the characteristic penetration depth which is wavelength dependent.

When the glass sample is thin, a small portion of the transmitted IR beam can be reflected from the backside of the sample and can be detected along with the beam reflected from the front

surface (Figure 1). In that case, the total reflectivity of SR-IR can be calculated as:

$$r_{p,121} = r_{p,12} + t_{p,12}r_{p,21}t_{p,21}e^{2i\beta} \text{ and } r_{s,121} = r_{s,12} + t_{s,12}r_{s,21}t_{s,21}e^{2i\beta} \quad (4)$$

where $t_{p,12}$ and $t_{s,12}$ is the transmission coefficients at the front surface for the beam entering from air, $r_{p,21}$ and $r_{s,21}$ is the reflection coefficient at the back surface, $t_{p,21}$ and $t_{s,21}$ is the transmission coefficient at the front surface for the beam reflected from the back surface, and $\beta = 2\pi b n_1 cos\theta_1/\lambda$ (where b = sample thickness; Figure 1) is the phase of the IR beam propagated through the glass. The transmission coefficients are calculated as:

$$t_{p,12} = \frac{2n_1 cos\theta_1}{n_2 cos\theta_1 + n_1 cos\theta_2} \text{ and } t_{s,12} = \frac{2n_1 cos\theta_1}{n_2 cos\theta_2 + n_1 cos\theta_1} \quad (5)$$

The $r_{p,21}$, $r_{s,21}$, $t_{p,21}$, and $t_{s,21}$ terms can be calculated by changing the subscript order in the $r_{p,12}$, $r_{s,12}$, $t_{p,12}$, and $t_{s,12}$ equations, respectively. Then, the total reflectance (R_{121}) from both front and back surfaces is calculated using the same equations (2) and (3) where $r_{p,121}$ and $r_{s,121}$, are used, instead of $r_{p,12}$ and $r_{s,12}$.

3. Results & Discussions

3.1 SR-IR and ATR-IR Spectra of Soda Lime Float Glass

Figure 3 compares the SR-IR and ATR-IR spectra of the soda lime float glass samples with 0.7 mm thickness. Two positive peaks at ~1064 cm^{-1} and ~766 cm^{-1} in SR-IR spectra in Fig. 3(a) are attributed to asymmetric and symmetric vibration modes of the Si-O-Si (BO) network

[3,8]. The shoulder at ~950 cm^{-1} corresponds to the stretching vibration of the $Si\text{-}O^-$ (NBO) group in the glass [3,4]. It is noted that the BO peak at ~1064 cm^{-1} appears to be missing or red-shifted to ~1000 cm^{-1} in the Ge-ATR spectrum and ~910 cm^{-1} in the diamond-ATR spectrum shown in Fig 3(b). ATR-IR also shows a broad peak spanning from 3650 cm^{-1} to ~2500 cm^{-1} corresponding to stretching vibrations of the hydrogen-bonded Si-OH and H_2O species, and a sharp peak at ~1650 cm^{-1} corresponding to the bending vibration of the molecular H_2O species. Although the ingress of water into the soda lime glass surface is true, it is incorrect to interpret the absence or red-shift of the BO peak in ATR-IR compared to the SR-IR as changes in the Si-O-Si network structure. This will be explained theoretically in the next section.

It is also noted that the SR-IR spectrum of 0.7mm thickness float glass collected at the 45^o incidence angle appears to show more spectral features than that of the same sample collected with the 15x objective lens in which the IR incidence angle is 20^o (Fig. 3(a)). The shoulder peak at ~1180 cm^{-1} and the negative peaks at ~2240 cm^{-1}, 2800 cm^{-1}, and 3500 cm^{-1} are observed only in the 45^o SR-IR spectrum, but not in the 20^o SR-IR spectrum. In the literature, the peak at 1180~1200 cm^{-1} has been attributed to a longitudinal optic (LO) mode of the network vibration [20,21]. The LO mode originates from the photon splitting in ionic crystals due to long-range Coulombic forces caused by ion motions during the vibrations [22]. In fact, this peak position is comparable to the value (~1250 cm^{-1}) reported for crystalline alpha-quartz [23]. The

LO mode can be observed only at oblique incidence angle with the *p*-polarized beam; but, it cannot be detected with the *s*-polarized beam since the electric field along the longitudinal direction is zero in the *s*-polarization [22]. Thus, without IR polarization-dependence measurement, one cannot ambiguously assign this peak to the LO mode. Also, the origin of the LO mode in amorphous glass is still unclear [24–27].

In Figure 3(a), the negative peaks at ~2240 cm^{-1}, ~2800 cm^{-1}, and ~3400 cm^{-1} of the θ_i=45^o spectrum could be puzzling since, as mentioned earlier, the absorption band in SR-IR should show up as a positive peak in the reflectance (R vs. cm^{-1}) plot. It is interesting to note that the peak positions of ~2800 cm^{-1} and ~3400 cm^{-1} agree well with the absorption bands in the transmission IR spectrum [28]. The ~2240 cm^{-1} is close to the peak reported for the Si-H (silane) group [29,30]. However, it should be noted that the peaks in SR-IR cannot be interpreted or assigned based on the coincidence of the SR-IR peak positions with the IR *absorption* bands of other materials.

3.2 Simulation of SR-IR and ATR-IR Spectra of Glass

In this section, the theoretical SR-IR and ATR-IR spectra are calculated using the equations (1) – (5) and the complex refractive index of diamond [17], germanium [18], and soda lime glass (Figure 2) [9], and compared with the experimental spectra shown in Figure 3. This comparison clearly shows that anomaly or artifacts of the SR-IR and ATR-IR spectra of glass

that should not be considered or interpreted as changes in absorption bands.

3.2a Comparison with simulated SR-IR spectra of glass

Figure 4 displays the calculated SR-IR spectra for soda lime glass. The simulated spectra clearly show that the peak shape and position vary with the IR incidence angle, as observed experimentally. At near normal incidences ($\theta_i \leq 20^o$), the peak shape is very similar to the shape of the imaginary part (k) of the complex refractive index. However, as θ_i increases to the oblique angle, the peak shape changes drastically and the position of the maximum intensity is also blue-shifted. The BO band position is shifted from ~1065 cm^{-1} at the near-normal incidence angle to ~1080 cm^{-1} at higher incidence angles. Note that his blue shift is not due to the changes in the strength or energy of the Si-O-Si bond (changes in the position of the $k(\lambda)$ maximum); it is simply due to the anomaly caused by the change in the real part of the refractive index, $n(\lambda)$ in the wavenumber region. The nearly zero reflectance at 1300 cm^{-1} is simply because the refractive index of glass is the same as that of air at this wavelength (see Figure 2).

It is noted that as the incidence angle increases, the peak near 1180~1200 cm^{-1} grows. In the previous literature, this peak has been ascribed to the LO mode [20,21]. If it is true LO mode, then it is expected to be detected only in the *p*-polarized spectrum but not in the *s*-polarized spectrum [22]. Figure 5 displays the *s*- and *p*-polarized spectra of the polished soda lime glass sample measured as a function of the angle of incidence. The growth of the 1180~1200 cm^{-1}

component is observed in both *s*- and *p*-polarized spectra. The simulated *s*- and *p*-polarized spectra from the refractive index shown in Figure 2 reproduced the same trend observed in the experimental data (insets of Figure 5). The small discrepancy in the peak shape must be due to the minor difference in the refractive index of the sample used in this study and the literature value shown in Figure 2. This comparison clearly shows that the growth of the 1180~1200 cm^{-1} component is due to the anomaly caused by the change in the real part (n) of the complex refractive index. This position coincides with the minimum of $n(\lambda)$ in Figure 2.

This simple theoretical calculation of the SR-IR spectra of glass demonstrates how the peak shape and position vary with the IR incidence angle due to the wavelength dependence of the refractive index. It is not due to the new vibration modes or absorption band at an oblique incidence angle. If new absorption bands are involved, then there should be new peaks in $k(\lambda)$; but, the simulated spectra shown in the insets of Figure 5 are all produced with the same $n(\lambda)$ and $k(\lambda)$ data set of soda lime glass (Figure 2).

In SR-IR analysis, the contribution from the backside reflection is sometimes ignored, which could lead to artifacts in the spectra. Figure 6(a) plots the IR penetration depth, d_p, calculated using $k(\lambda)$ in Figure 2. The penetration depth varies from ~0.65 μm at the BO absorption band position to ~2 cm in the >3700 cm^{-1} region. It is noted that when the sample thickness is 700 μm, then the >2200 cm^{-1} region of the IR beam can be reflected from the

backside of the glass sample. This backside reflection can contribute to the signal intensity in the SR-IR experiment. When a microscope objective lens is used (θ_i=20^o data shown in Figure 3(a)), the backside reflection is negligible since the focal depth of the objective lens is only on the order of several microns. However, in the typical SR-IR experiment with an elliptical mirror with a long focal distance (θ_i=45^o data shown in Figure 3(a)), the backside reflection should be taken into account.

Figure 6(b) shows how the backside reflection alters the SR-IR spectrum of a 700 μm thick float glass sample. When the IR beam is reflected from the front surface only, the SR-IR spectrum has no features at λ > 2000 cm^{-1}. The reflection from the backside has zero signal at λ < ~2240 cm^{-1}, but has non-zero signal at λ > ~2240 cm^{-1}. Since the front and backside reflected beams are spatially separated, the interference effect is negligible and the signals from these surfaces can be added. When these two components are added, the sum spectrum (solid line in Figure 6(b)) shows negative peaks at ~2240 cm^{-1}, ~2800 cm^{-1}, and ~3400 cm^{-1}, which is in good agreement with the experimentally observed spectrum (Figure 3(a), inset). This simulation clearly explains that the *apparent* peak at ~2240 cm^{-1} should not be interpreted as the silane (Si-H) species in the soda lime glass; it is simply the *onset* of the backside reflection contribution in SR-IR of a thin optically-flat glass sample. Note that the Si-H peaks are normally very sharp. The negative peaks at ~2800 cm^{-1} and 3400 cm^{-1} in the SR-IR spectrum are due to the absorption

by hydrous species in the bulk. In this sense, the region above ~2240 cm^{-1} in the SR-IR spectrum is similar to the transmission absorption spectrum.

In order to further understand the backside reflection contribution in SR-IR, we conducted a few control experiments (Figure 6(c)). When the sample thickness is changed from 700 μm to 5mm, then the onset of the backside contribution is shifted from ~2240 cm^{-1} to ~3600 cm^{-1}. When the backside of the 5mm thick sample is roughened, then this contribution is further suppressed. When CCl_4 is placed on the back of the 700 μm thick sample, then the backside reflection is completely suppressed since the refractive index of CCl_4 is very close to that of soda lime glass.

3.2b Comparison with simulated ATR-IR spectra of glass

In ATR-IR, the IR incident beam travels through the high refraction index crystal and is reflected from the crystal/glass interface; thus, the reflection behavior can be divided into two regimes: (i) $\theta_i < \theta_c$ (SR-IR region) and (ii) $\theta_i > \theta_c$ (ATR-IR region). The critical angle (θ_c) is ~38.7^o for the diamond crystal and ~22.0^o for the germanium crystal. When $\theta_i < \theta_c$, the peak shapes in the reflection spectra shown in Figures 7(a) and 7(b) appear to be governed mostly by the real part, $n(\lambda)$, of the glass refractive index (Figure 2). When $\theta_i > \theta_c$, the signal in the non-absorbing region (>1200 cm^{-1}) is almost zero since the IR beam undergoes total internal reflection (i.e., $R = I_r/I_o = 1$; $\log(1/R) \approx 0$). In the absorbing region (<1200 cm^{-1}), $k(\lambda)$ has

non-zero value and the total internal reflection is attenuated (i.e., R < 1; log(1/R) > 0). It is noted that the Si-O-Si peak position of the maximum intensity is not the same as the absorption band position in $k(\lambda)$; it is significantly red-shifted to ~910 cm^{-1} for the diamond-ATR data in Figure 7(a) and ~990 cm^{-1} for the Ge-ATR data in Figure 7(b). Such a red-shift in the absorption peak position is insignificant for organic materials since $k(\lambda)$ is very small and thus variance in $n(\lambda)$ is negligible. However, in the case of soda lime glass, both $n(\lambda)$ and $k(\lambda)$ vary over a large range, causing distortion of the peak shape in the ATR-IR spectrum. Thus, the difference in the peak positions of the SR-IR and ATR-IR spectra should not be interpreted as structural modification in the surface region [12]. These differences are simply due to the anomaly of the IR beam reflection resulting from changes in $n(\lambda)$.

3.3 SR-IR vs. ATR-IR for Study of Si-O-Si Network Structure

The leaching of sodium via acid treatment is usually observed to shift and alter the shape of the broad band in the 1200 – 850 cm^{-1} region [3]. Figure 8 compares the changes observed in the SR-IR and Ge ATR-IR spectra of the acid-treated soda lime glass surfaces. In the SR-IR spectra (Figure 8(a)), it can be seen that, upon acid treatments, the peak position of the BO band is slightly blue-shifted (from 1054 cm^{-1} to 1060 cm^{-1}) and the intensity of the NBO region (shoulder peak at ~950 cm^{-1}) is slightly increased. The change in the NBO region can be attributed to conversion of the NBO group to the Si-OH species upon leaching of Na^{+} into

solution and ingress of H^+ from the solution. Most divalent Ca^{2+} and Mg^{2+} ions remained in the surface region after leaching since they have less mobility than Na^+ [31]. Therefore, they have less effect on the peak position compared with leaching of Na^+. The glass samples also contain several hundred ppm of iron. Even if its oxidation state could be changed, its impact is negligible since its concentration is too low [32].

The Ge ATR-IR spectra (Figure 8(b)) show larger blue-shift of the main peak from 990 cm^{-1} to 1010 cm^{-1}. And the intensity of the 950 cm^{-1} region decreases with acid treatment, which is opposite to the trend seen in SR-IR. One may attempt to interpret this observation in conjunction with the difference in the information depth of two methods: d_p = 650 nm at 1060 cm^{-1} in SR-IR and 490 nm at 1000 cm^{-1} in Ge ATR-IR. However, it should be noted that the peak shape and position of the Ge ATR-IR spectrum implies that the ~1000 cm^{-1} peak are affected by the convolution of $n(\lambda)$ and $k(\lambda)$. In other words, the anomaly effect of the complex refractive index of glass made the blue-shift larger in the Ge ATR-IR spectra, compared to the SR-IR spectra.

In the case of the diamond ATR-IR analysis, the peak position of the 910 cm^{-1} band (Figures 2(b) and 7(a)) was blue-shifted by +1 cm^{-1} after 20 hours of acid etching and then red-shifted by -2 cm^{-1} after 320 hours (data not shown). This difference in the peak position change upon the acid etching treatment reiterated that the peaks in the Si-O-Si vibration region

of the ATR-IR spectra of glass samples are altered by the anomaly effect originating from the complex refractive index of glass.

3.5 Diamond vs. Germanium ATR-IR for Detection of Hydrous Species

ATR-IR can be used to probe the hydrous species in the near surface region of soda lime glass [14,15]. The broad band within the 3800-2500 cm^{-1} region can be attributed to the OH stretching vibrations of Si-OH and H_2O species with varying degrees of hydrogen bonding interactions. Note that the 3450-3200 cm^{-1} region overlaps with the OH stretch vibrations of molecular water species in liquid or adsorbed layers;[33] but this does not mean that all peaks in the region can be assigned to the molecular water. The OH stretch peak of molecular water as well as Si-OH could overlap depending on the degree of hydrogen bonding interactions.[34] The presence of the H-O-H bending vibration peak at ~1650 cm^{-1} indicates the presence of molecular water in the ATR-IR probe depth. Both Ge and diamond ATR-IR spectra clearly show these peaks (Figure 9(a) and (b)). Since the absorptivity of glass itself in this region is very small, the observed peaks can be interpreted as absorption bands of the Si-OH and H_2O species as in the case of transmission analysis.

However, the interpretation of the peak intensity is not as straightforward as the transmission analysis [15,35]. In Figure 9(c), the increases of the 3400cm^{-1} peak intensity after acid treatment are plotted as a function of the hydrogen amount in the samples surface calculated

from SIMS data reported elsewhere[15]. In both diamond and Ge ATR-IR, the signal intensity increases non-linearly with the hydrogen amount. This is because the electric field of the evanescence wave decreases exponentially as a function of distance from the surface and contribution to signal intensity by absorption in deeper region are weakened due to its attenuation. It is noted that the signal intensity is much weaker in the Ge ATR-IR spectra compared to the diamond ATR-IR spectra. This is mainly due to the difference in the penetration of the evanescent wave. The penetration depth ($d_{p,ATR}$) at 3400 cm^{-1} is calculated to be 600 nm for diamond ATR and 150 nm for Ge ATR. Thus, the Ge ATR-IR signal becomes saturated much faster than the diamond ATR-IR signal.

4. Conclusions

Infrared spectroscopy is an important and valuable tool for the characterization of glass structure, water in glass and water adsorption/reaction at surfaces. Although the fundamental vibrational state of the material is the desired information in all of these methods, the position, shape and intensity of the measured absorption peaks are influenced and sometimes distorted by differences and anomalies associated with how the data is acquired. In this study, SR and ATR have been used to acquire spectra of a commercial soda lime float glass, to describe and analyze the associated spectral features in detail. The observed differences in the wavenumber and shape

of the important peaks for each mode of data acquisition are explained using classical optical theory. The effects of incidence angle, backside reflections and information depth are highlighted. For example, the Si-O-Si BO peak is blue-shifted in SR-IR and red-shifted in ATR-IR simply due to the complex nature of the glass refractive index, not due to differences in probe depth. Likewise, the growth of a peak at ~1200 cm^{-1} in SR-IR at oblique angles cannot be attributed to the LO mode of the Si-O-Si vibration. In the case of thin and flat glass samples, the IR reflection from the back surface can superimpose the transmission spectrum on the SR-IR spectrum in the wavenumber region where the bulk absorption coefficient is low. The effect of acid leaching on the Si-O-Si BO network should be analyzed by SR-IR, not by ATR-IR. When the ATR-IR intensity of the hydrous peaks (Si-OH and H_2O) is interpreted, the inhomogeneous in-depth profile of the hydrogen and the IR penetration depth must be taken into account.

Acknowledgements. This work was supported by the National Science Foundation (Grant No. DMR-1207328). S. Amma was supported by Asahi Glass Co.

References

[1] L.C. Bradley, Z.R. Dilworth, A.L. Barnette, E. Hsiao, A.J. Barthel, C.G. Pantano, et al., Hydronium ions in soda-lime silicate glass surfaces, J. Am. Ceram. Soc. 96 (2013) 458–463. doi:10.1111/jace.12136.

[2] H. He, L. Qian, C.G. Pantano, S.H. Kim, Mechanochemical wear of soda lime silica glass in humid environments, J. Am. Ceram. Soc. 97 (2014) 2061–2068. doi:10.1111/jace.13014.

[3] F. Geotti-Bianchini, L. De Rui, G. Gagliardi, M. Guglielmi, C.G. Pantano, New interpretation of the IR reflectance spectra of SiO2 rich films on soda lime glass, Glas. Berichte. 64 (1991) 205–217.

[4] F. Geotti-Bianchini, M. Preo, M. Guglielmi, C.G. Pantano, Infrared reflectance spectra of semi-transparent SiO2 rich films on silicate glasses: Influence of the substrate and film thickness, J. Non. Cryst. Solids. 321 (2003) 110–119. doi:10.1016/S0022-3093(03)00154-6.

[5] N.J. Smith, C.G. Pantano, Leached layer formation on float glass surfaces in the presence of acid interleave coatings, J. Am. Ceram. Soc. 91 (2008) 736–744. doi:10.1111/j.1551-2916.2007.02079.x.

[6] R.M. Almeida, T.A. Guiton, C.G. Pantano, Characterization of silica gels by infrared reflection spectroscopy, J. Non. Cryst. Solids. 121 (1990) 193–197. doi:http://dx.doi.org/10.1016/0022-3093(90)90130-E.

[7] M. Tomozawa, Y. Lee, Surface fictive temperature of annealed and rate-cooled soda lime glasses, J. Non. Cryst. Solids. 253 (1999) 119–125.

[8] T. Uchino, T. Sakka, M. Iwasaki, Interpretation of Hydrated States of Sodium Silicate Glasses by Infrared and Raman Analysis, J. Am. Ceram. Soc. 74 (1991) 306–313. doi:10.1111/j.1151-2916.1991.tb06880.x.

[9] M. Rubin, Optical properties of soda lime silica glasses, Sol. Energy Mater. 12 (1985) 275–288. doi:10.1016/0165-1633(85)90052-8.

[10] A.B. Kuzmenko, Kramers-Kronig constrained variational analysis of optical spectra, Rev. Sci. Instrum. 76 (2005) 1–9. doi:10.1063/1.1979470.

[11] S. a Macdonald, C.R. Schardt, D.J. Masiello, J.H. Simmons, Dispersion analysis of FTIR reflection measurements in silicate glasses, J. Non. Cryst. Solids. 275 (2000) 72–82. doi:10.1016/S0022-3093(00)00121-6.

[12] T. Uchino, T. Sakka, K. Hotta, M. Iwasaki, Attenuated Total Reflectance Fourier-Transform Infrared Spectra of a Hydrated Sodium Silicate Glass, J. Am. Ceram. Soc. 72 (1989) 2173–2175.

[13] H. Hosono, Fourier transform infrared attenuated total reflection spectra of ion-implanted silica glasses, J. Appl. Phys. 69 (1991) 8079. doi:10.1063/1.348925.

[14] J.B. Lowenstern, B.W. Pitcher, Analysis of H2O in silicate glass using attenuated total reflectance (ATR) micro-FTIR spectroscopy, Am. Mineral. 98 (2013) 1660–1668. doi:10.2138/am.2013.4466.

[15] S. Amma, S.H. Kim, C.G. Pantano, Analysis of Water and Hydroxyl Species in Soda Lime Silica Glass Surfaces using Attenuated Total Reflection (ATR) - IR spectroscopy, J. Am. Ceram. Soc. (2015).

[16] M.E. Pemble, P. Gardner, Infrared Spectroscopy from Surfacese, in: J.C. Vickerman, I.S. Gilmore (Eds.), Surf. Anal. – Princ. Tech., 2nd Editio, John Wiley & Sons, Ltd, Chichester, West Sussex, PO19 8SQ, United Kingdom, 2009: pp. 334–361.

[17] A.M. Zaitsev, Optical properties of diamond, A data handbook, Springer, 2011.

[18] N.P. Barnes, M.S. Piltch, Temperature-dependent Sellmeier coefficients and nonlinear optics average power limit for germanium, J. Opt. Soc. Am. 69 (1979) 178. doi:10.1364/JOSA.69.000178.

[19] M. Milosevic, Internal Reflection and ATR Spectroscopy, First Edit, Wiley & Sons, Inc., Hoboken. New Jersey, 2012.

[20] F.L. Galeener, G. Lucovsky, Longitudinal Optical Vibrations in Glasses: GeO2 and SiO2, Phys. Rev. Lett. 37 (1976) 1474–1478.

[21] R.M. Almeida, Detection of LO modes in glass by infrared reflection spectroscopy at oblique incidence, Phys. Rev. B. 45 (1992) 161–170.

[22] M.D. Sciacca, A.M. Mayur, E. Oh, A.K. Ramdas, S. Rodriguez, J.K. Furdyna, et al., Infrared observation of transverse and longitudinal polar optical modes of semiconductor films: Normal and oblique incidence, Phys. Rev. B. 51 (1995) 7744–7752.

[23] J.F. Scott, S.P.S. Porto, Longitudinal and Transverse Optical Lattice Vibrations in Quartz, Phys. Rev. 161 (1967) 903–910.

[24] S.W. de Leeuw, M.F. Thorpe, Coulomb splittings in glasses, Phys. Rev. Lett. 55 (1985) 2879–2882.

[25] C.T. Kirk, Quantitative analysis of the effect of disorder-induced mode coupling on infrared absorption in silica, Phys. Rev. B. 38 (1988) 1255–1273.

[26] J. Sarnthein, A. Pasquarello, R. Car, Origin of the High-Frequency Doublet in the Vibrational Spectrum of Vitreous SiO2, Science (80-.). 275 (1997) 1925–1927. doi:10.1126/science.275.5308.1925.

[27] A. Pasquarello, R. Car, Dynamical Charge Tensors and Infrared Spectrum of Amorphous SiO2, Phys. Rev. Lett. 79 (1997) 1766–1769. doi:10.1103/PhysRevLett.79.1766.

[28] P.B. McGinnis, J.E. Shelby, Diffusion of water in float glass melts, J. Non. Cryst. Solids. 177 (1994) 381–388. doi:10.1016/0022-3093(94)90552-5.

[29] J.E. Shelby, Protonic species in vitreous silica, J. Non. Cryst. Solids. 179 (1994) 138–147. doi:10.1016/0022-3093(94)90691-2.

[30] J.E. Shelby, Water in glasses and melts, in: Introd. to Glas. Sci. Technol., 2nd Editio, The Royal Society of Chemistry, Cambridge, UK, 2005: pp. 222–236.

[31] F. V Natrup, H. Bracht, S. Murugavel, B. Roling, Cation diffusion and ionic conductivity in soda-lime silicate glasses., Phys. Chem. Chem. Phys. 7 (2005) 2279–2286. doi:10.1039/b502501j.

[32] E.. Boulos, L.. Glebov, T.. Smirnova, Absorption of iron and water in the Na2O–CaO–MgO–SiO2 glasses. I. Separation of ferrous and hydroxyl spectra in the near IR region, J. Non. Cryst. Solids. 221 (1997) 213–221. doi:10.1016/S0022-3093(97)00334-7.

[33] D.B. Asay, S.H. Kim, Evolution of the adsorbed water layer structure on silicon oxide at room temperature., J. Phys. Chem. B. 109 (2005) 16760–3. doi:10.1021/jp053042o.

[34] A. Novak, Hydrogen bonding in solids correlation of spectroscopic and crystallographic data, in: Large Mol. SE - 4, Springer Berlin Heidelberg, 1974: pp. 177–216. doi:10.1007/BFb0116438.

[35] M. Milosevic, Depth Profiling, in: Internal Reflection and ATR Spectroscopy, First Edit, Wiley & Sons, Inc., Hoboken, New Jersey, 2012: pp. 92–96.

Figures

Figure 1.

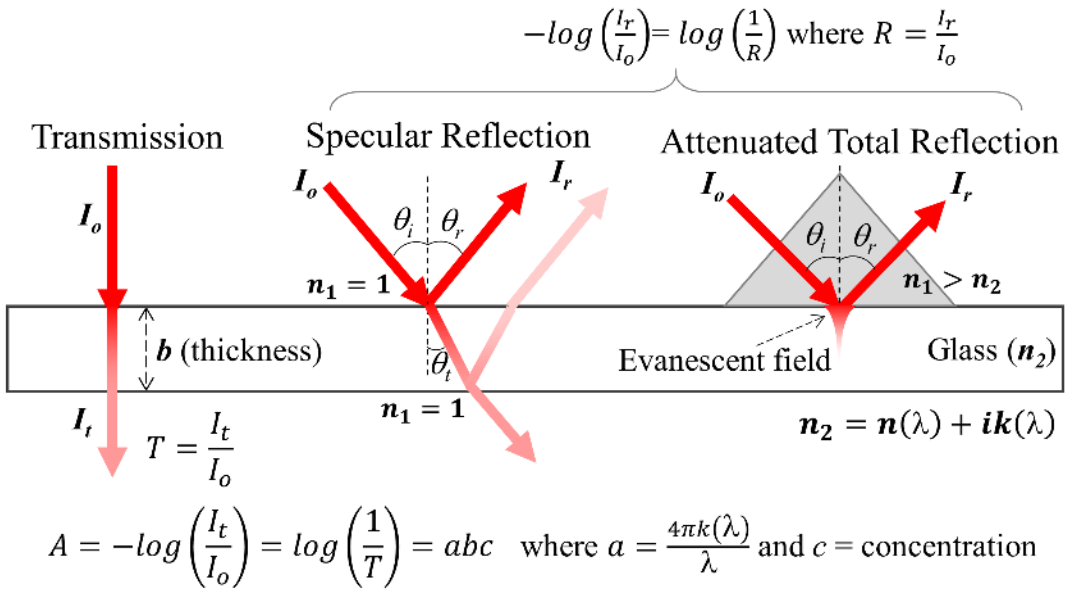

Figure 2.

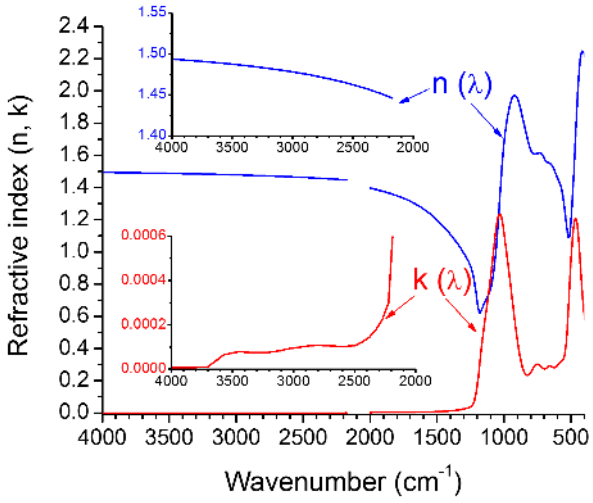

Figure 3.

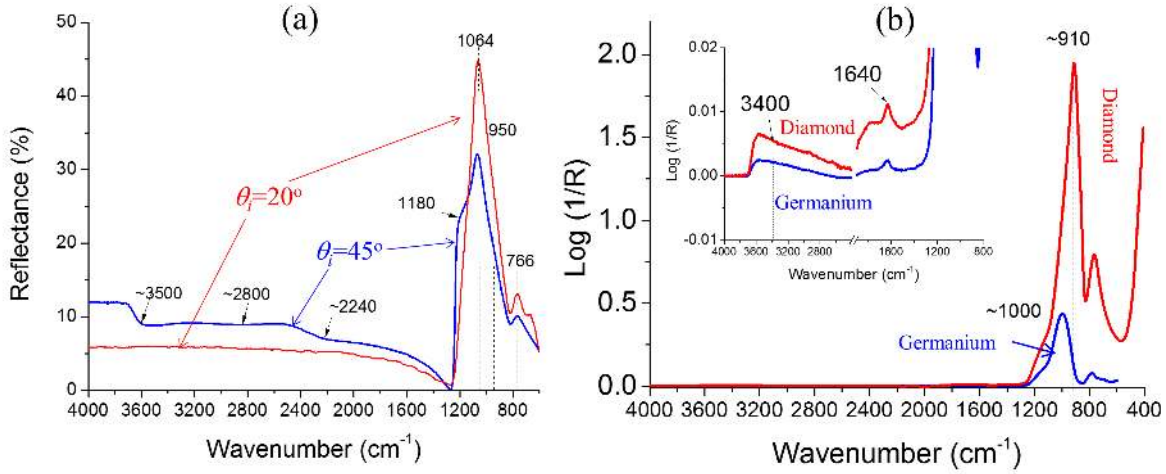

Figure 4.

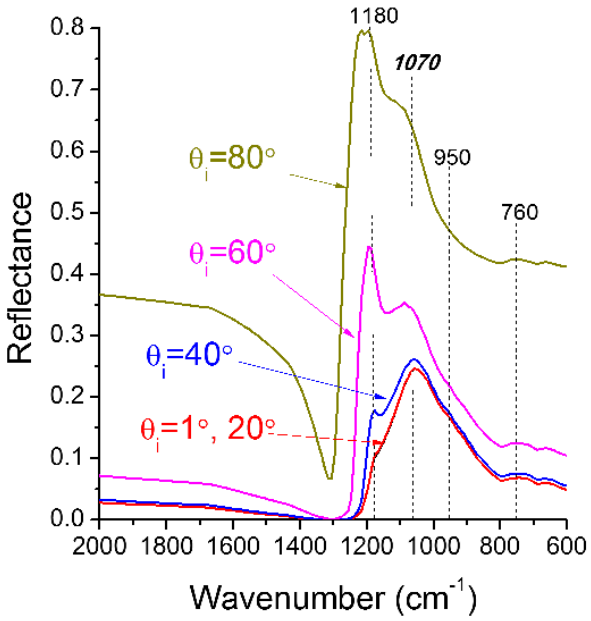

Figure 5.

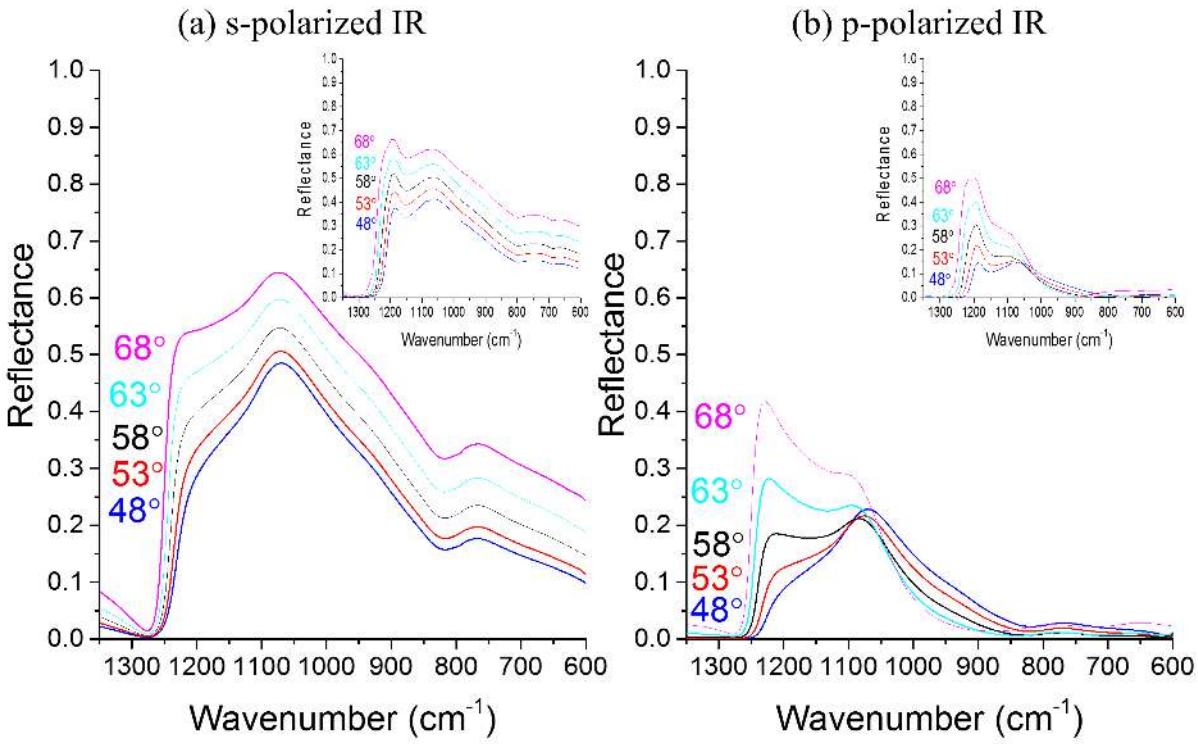

Figure 6.

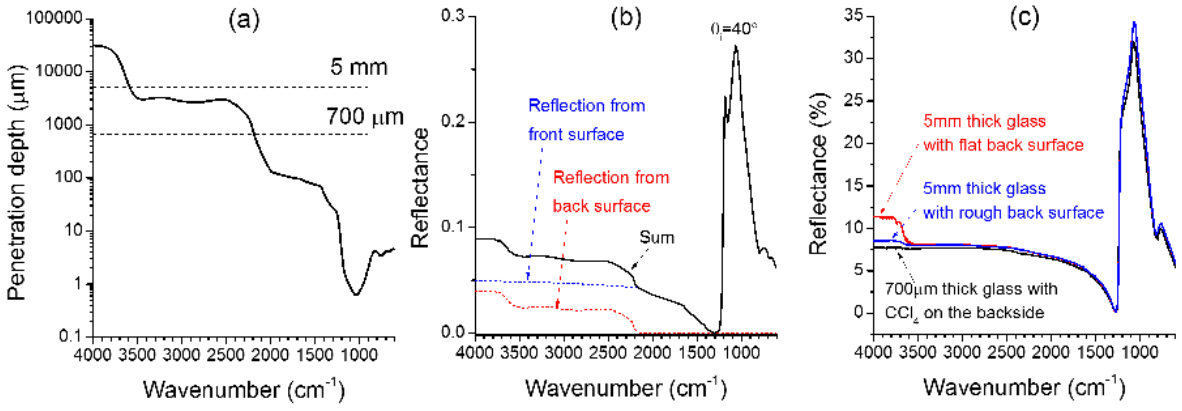

Figure 7.

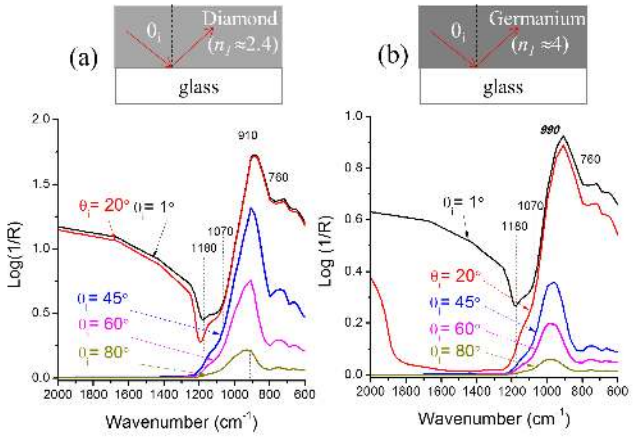

Figure 8.

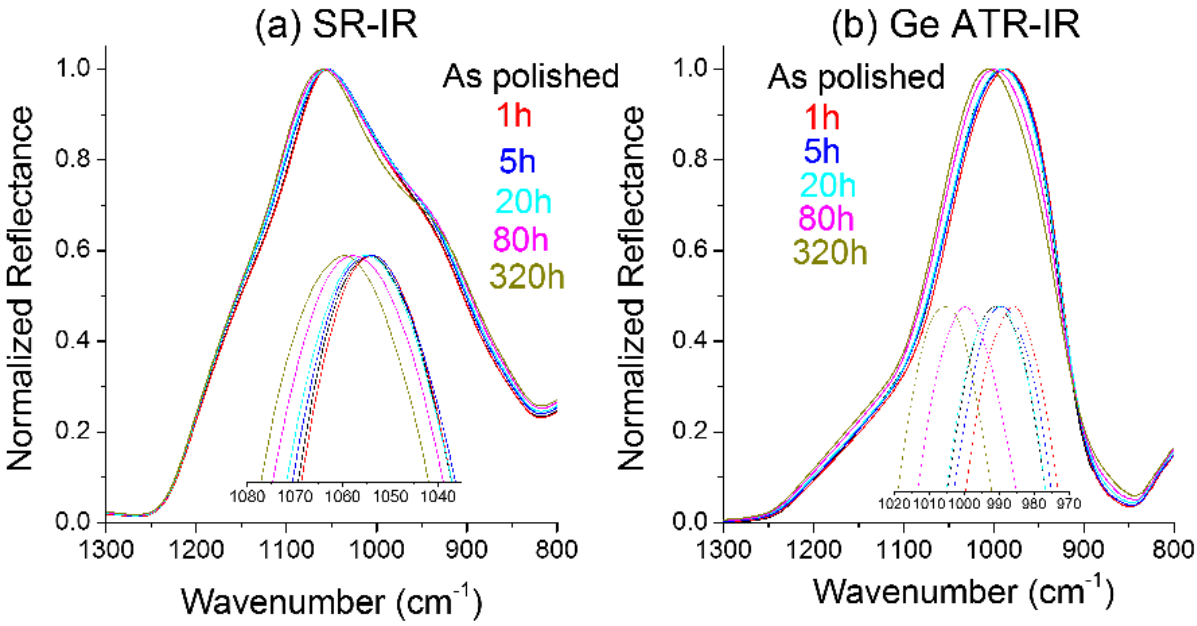

Figure 9.

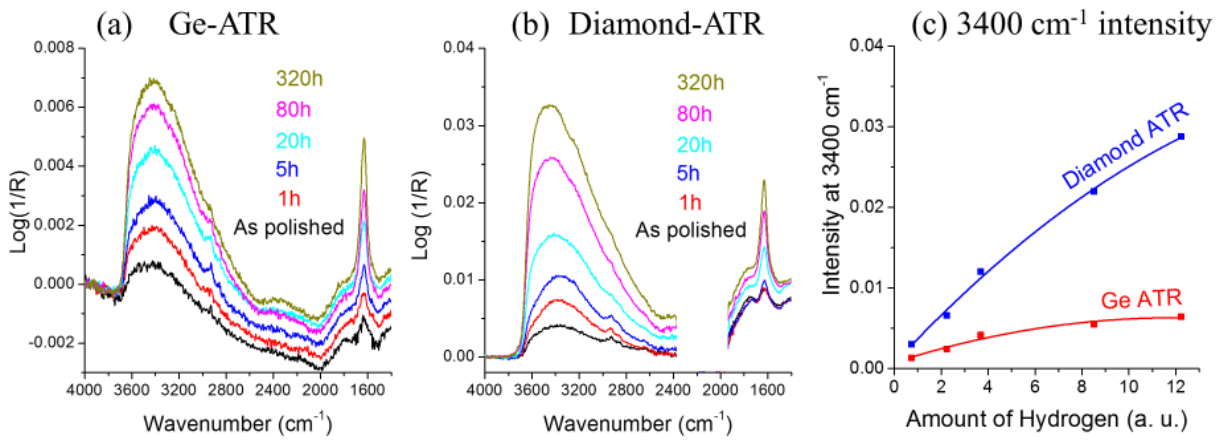
(a) Ge-ATR
320h
80h
20h
5h
1h
As polished
Log(1/R)
Wavenumber (cm-1)
(b) Diamond-ATR
320h
80h
20h
5h
1h
As polished
Log (1/R)
Wavenumber (cm-1)
(c) 3400 cm-1 intensity
Diamond ATR
Ge ATR
Intensity at 3400 cm-1
Amount of Hydrogen (a. u.)

Table Captions

Table 1. Glass composition evaluated by XRF

Figure Captions

Figure 1. Schematic illustration of transmission, specular reflection (SR), and attenuated total reflection (ATR) IR spectroscopy of a flat glass sample.

Figure 2. Real (n) and imaginary (k) components of refractive index of soda lime glass.[9]

Figure 3. (a) SR-IR spectra of soda lime float glass with 0.7 mm thickness obtained at an incidence angle of 20^{o} (with a 15x IR objective lens) and 45^{o}. The inset shows the 4000 – 1600 cm^{-1} region of the 45^{o} incidence angle spectrum. (b) ATR-IR spectra of soda-lime float glass with 0.7 mm thickness obtained with diamond and Ge ATR crystals. The inset shows the 4000 – 1200 cm^{-1} region of the ATR-IR spectra.

Figure 4. SR-IR spectra of soda lime glass calculated with eqs. (1) – (3) using the refractive index shown in Figure 2 at different incidence angles (θ_i).

Figure 5. Comparison of (a) s-polarized and (b) p-polarized SR-IR spectra of polished soda lime glass at incidence angles θ_i at the Brewster angle (58^{o}) as well as $\pm5^{o}$ and $\pm10^{o}$. The main panels are the experimental spectra and the insets are the spectra simulated with eqs. (1) – (3) using the

refractive index shown in Figure 2.

Figure 6. (a) IR penetration depth, d_p, inside soda lime glass calculated with $k(\lambda)$ shown in Figure 2. (b) SR-IR spectrum calculated for a 700 μm thick soda lime glass using equations (1) – (5) at an incidence angle of 40^o. The dotted lines are the components calculated for the reflection from the front and back surfaces. (c) Experimentally obtained SR-IR spectra of soda lime glass with different backside reflection conditions.

Figure 7. (a) Diamond ATR-IR, and (b) Ge ATR-IR spectra of soda lime glass calculated with eqs. (1) – (3) using the refractive index shown in Figure 2 at different incidence angles (θ_i). Note that the calculated spectra for $\theta_i = 1^o$ and 20^o correspond to the SR-IR data since the incidence angle is lower than the critical angle (θ_c).

Figure 8. (a) SR-IR ($\theta_i = 20^o$) and (b) Ge ATR-IR spectra of acid-treated soda lime glass samples for 0, 1, 5, 20, 80, and 320 hours.

Figure 9. ATR-IR spectra of acid-treated soda lime glass surfaces obtained with (a) germanium and (b) diamond crystals. (c) Comparison of the 3400 cm^{-1} peak intensity with the hydrogen amount in the glass surface. The hydrogen amount on the x-axis is adapted from the secondary ion mass spectrometry analysis (SIMS) result reported in ref. [15].